
ASSESSING CAUSAL EFFECTS OF INTERVENTIONS IN TIME USING GAUSSIAN PROCESSES

Gianluca Giudice, Sara Geneletti and Konstantinos Kalogeropoulos

Department of Statistics

LSE

g.giudice@lse.ac.uk; k.kalogeropoulos@lse.ac.uk; s.geneletti@lse.ac.uk;

October 7, 2022

1 Introduction

Recently, many applications have been devoted to understanding and revealing *causal* rather than associative relations among variables. One approach in the context of time series is that of synthetic controls (Abadie and Gardeazabal, 2003) and various extensions. This is based on the idea of recovering the counterfactual outcome that would have been observed had an intervention not taken place.

This article contributes to expanding and generalizing this class of models, allowing for non-linearity in a non-parametric manner through Gaussian Processes. These models have high degree of flexibility in building the counterfactual outcome, using all types of information and without any limitations on the functional form. They also make it possible to assess the robustness of the synthetic controls, as we can use the posterior distributions of the Gaussian Processes to quantify uncertainty stemming from the functional form estimation. Lastly, as the models learn the relationships which prevail amongst all associated variables, there is no need to match the time series on a calendar basis, making the most of the available data.

To our best knowledge the only paper that uses Gaussian process in the context of potential outcomes is Alaa and van der Schaar (2017). The purpose of the article was to infer individualized treatment effects across a series of cross sectional experiments. However, the bivariate setting arises from the use of the treated and control group as dependent variables and no time component is exploited. There exists very recent literature that explores multi task causal learning using Gaussian process exploiting Judea Pearl's Do-Calculus (Pearl, 1995). These papers (Aglietti et al., 2020) however are mainly focused on understanding the main correlation structure of multiple continuous intervention functions - defined with a directed acyclic graph (DAG) - as opposed to a single discrete intervention. Furthermore, the main data domain consist of cross sectional experiments, not time series data.

This paper is structured as follows. In section 2 we briefly introduce the causal framework and the synthetic

control approach, presenting our main assumptions and the causal effect estimands. In Section 3 we define the proposed models based on Gaussian Processes. In Section 4, we present the estimation procedure. In Section 5 we present an illustrative empirical analysis of our approach to obtain estimates of the causal effect of the UK's effective vaccination programme, introduced in January 2021, on deaths and infection rate. Section 6 describe the main results of the analysis. Finally, we conclude in section 7.

2 Background

The application we refer to throughout the paper serves as an illustrative example and is analysed in Section 5. It attempts to understand whether the early and intense vaccination campaign introduced in the UK affected the number of deaths and level of contagiousness of Covid-19 in the first semester of 2021. Formally, the treated unit is the UK and the treatment is the substantially accelerated vaccination schedule. Other EU countries, with other slower vaccination campaigns will be used to construct the synthetic control for the UK. We would like to note here that we are comparing the UK with a non-treated counterfactual version of itself, using other European countries to create this counterfactual.

Each observation is denoted with $y_{i,t} \in \mathcal{Y}$, where $i = 1, \dots, m$ is reserved for countries and $t = 1, \dots, T_i$ for observation times, is associated with a set of d potentially time-varying predictors $\mathbf{x}_{i,t} \in \mathcal{X}^d$ such that

$$y_{i,t} = f(\mathbf{x}_{i,t}) + \epsilon_{i,t}, \quad \epsilon_{i,t} \sim \mathcal{N}(0, \omega_i^2),$$

where $f(\cdot)$ is a generic function which express the input-output relationship and $\epsilon_{i,t}$ is the error term, having mean 0 and variance ω_i^2 . The d -dimensional feature vector $\mathbf{x}_{i,t}$ is a set of time series specific to each unit i . In our application this includes mobility data and number of tests for each country. The data span T_i periods and the first t_0 periods correspond to the data before the intervention, i.e. when the vaccination campaign began in the UK.

2.1 Synthetic Control Methods

Synthetic control methods have gained traction as methods to estimate causal effects from variables that were subject to a single intervention or treatment in time. A traditional approach is the one based on the *difference-in-difference* (DD) method, a static linear regression model where the causal effect is estimated as the difference between the regression coefficient in the treated and the control group. This is often implemented in a linear regression setting, with the quantity of interest being the interaction term of the dependent variable and the treatment group dummy variable. In this case, $f(\mathbf{x}_{i,t}) = \alpha + \mathbf{x}_{i,t}'\beta + \gamma D(t_0)$, where $D(t_0)$ is a dummy variable which take values 1 for $t > t_0$ and α, β, γ are the ordinary least square coefficients. However, DD methods suffer from two main drawbacks (Brodersen et al., 2014): the first one is that it assumes that the data are independent and identically distributed, thus disregarding the temporal component; secondly, the pre and post intervention periods are captured solely by two time points Abadie et al. (2010) Abadie and Gardeazabal (2003) proposed models generalizing the DD as they allowed the effect of unit-specific unobserved variables to vary with time. In particular, they recover the counterfactual outcome by developing a control group that has a similar pattern in the pre-intervention period as the treated unit. To do so they find a vector of weights $\{W_1, \dots, W_{m-1}\}'$, $W_j > 0$, $\sum W_j = 1$ which minimize the squared distance between the pre-intervention features (not time series) of the exposed region \mathbf{x}_i and the features for the unaffected regions $\{\mathbf{x}_j\}_{j \neq i}$. Then, the counterfactual outcome becomes $y_{i,t} = \sum_{j \neq i} W_j y_{j,t}$. However, this method has its own limitations. Indeed, it focuses only on possible convex combinations of control time series to match the treated

variable. Furthermore, there is a non-negligible data loss in regards to the temporal component. First of all, only data in the pre-treatment period is used to fit the model and find the optimal weights of the counterfactual unit. Second, time series evolution and interaction over time is neglected, as data is aggregated over time or treated individually for each time period. An alternative class of models is identified by Brodersen et al. (2014), whose approach addresses many of the previous methods limitations. The authors approach relies on Bayesian state space models which encompass the outcome's temporal evolution with exogenous regression components to efficiently build a counterfactual model. State space models allow for flexibility when modelling a variable that is affected by external noise, distinguishing between a state equation which describe the transition of the latent variable from one point in time to the next one, and a measurement equation, which describes the accuracy of the signal¹. Being fully Bayesian makes it possible to (i) incorporate prior information about the model structures and parameters and (ii) have a posterior distribution, and thus a probabilistic uncertainty quantification of the causal impact of the intervention. Although the models focus on one outcome variable and multiple controls, an extension to a multivariate setting has been implemented using Multivariate Bayesian Structural Time Series (Menchetti and Bojinov, 2020), which is limited to linear relationships between outcomes and controls and subject to the Markovian assumption of the variables.

2.2 Assumptions

In this subsection, we set up the framework to estimate the causal effect of an intervention on the treated subject. Each subject $y_{i,t}$, i.e. each country in our application, is associated with a binary potential outcome $y_{i,t}(w_{i,t}) \in \mathbb{R}$ where $w_{i,t} \in \{0, 1\}$ is a treatment assignment indicator with '1' referring to the variable being treated (the UK) and '0' to the controls (other European countries). Furthermore, define $\mathbf{w}_{1:m,1:T} = \{\mathbf{w}_{1,1:T}, \dots, \mathbf{w}_{m,1:T}\}$ as the assignment path up to time T of all units $i = 1, \dots, m$ and denote $\mathbf{w}_{1:m,1:T}$ a realization of this path. As in Menchetti et al. (2021), throughout the paper we make a set of assumptions to guarantee that the differences in the potential outcome trajectories are a direct statistical consequence of the intervention. Since some of them can not be directly tested, we rely on the concept of *plausibility* in our empirical settings. In particular, we assume the following:

Assumption 1 (Single intervention) *Unit i received a single intervention if there exist a $t_0 \in \{1, \dots, T\}$ such that $w_{i,t} = 0$ for all $t < t_0$ and $w_{i,t} = w_{i,s} = w_i$ for all $t, s > t_0$.*

This says that the treatment is single, i.e. it occur at one point in time, and is persistent, i.e. has no disruptions. Then, we can ease the notation and drop the t subscript for $t > t_0$

Assumption 2 (Temporal no-interference) *For all for all $i \in \{1, \dots, m\}$ and all $t > t_0$, the outcome of unit i at time t depends only on its own treatment path*

$$y_{i,t}(\mathbf{w}_{1:m,t_0+1:T}) = y_{i,t}(\mathbf{w}_{i,t_0+1:T})$$

If it holds, one can drop also the subscript i from \mathbf{w}_i as this assumption asserts that whether or not other units receive the treatment at time t_0 , this has no impact on other units' potential outcome. Units do not interfere with each other at any point in time. This is the time series equivalent of the cross-sectional Stable Unit Treatment Value Assumption (SUTVA) Rubin (1974) also known as Temporal SUVTVA from the work of Bojinov and Shephard (2019). In our

¹Formally, dropping the subscript i , $y_t = Z' \alpha_t + \gamma \mathbf{x}_t + \epsilon_t$ represent the *observation equation* and $\alpha_{t+1} = \Phi \alpha_t + R \eta_t$ is the *state equation*, where $\epsilon_t \sim \mathcal{N}(0, \sigma_\epsilon^2)$ and $\eta_t \sim \mathcal{N}(0, \sigma_\eta^2)$. See Brodersen et al. (2014) for more details

empirical study, each countries vaccination plan is confined by the country's border and does not affect other countries rate of contagion or number of deaths. The main underlying observation around this assumption is that, during the period analysed, each country was isolated due to government restriction. Thus, people mobility was prohibited or at least significantly limited. Even after the intervention, we likely expect other European countries mobility not to affect the UK number of deaths or contagion rate.

Assumption 1 and 2, allow as to simplify the notation so that we can use $y_{i,t}(w)$ to indicate the potential outcome of a generic unit i at time t . Thus, the observed outcome for $t > t_0$ is $y_{i,t}(1)$ while $y_{i,t}(0)$ is the *unobserved* or *counterfactual* potential outcome which has to be estimated to measure the causal impact of the intervention.

Assumption 3 (Covariates-treatment independence) *Denote $\mathbf{x}_{i,t}$ the vector of exogenous variable that are predictive of $y_{i,t}$. For $t > t_0$ those covariates are not affected by the intervention*

$$\mathbf{x}_{i,t}(1) = \mathbf{x}_{i,t}(0)$$

These covariates help improve the outcome prediction but they produce an estimation bias if they are influenced by the treatment. For the analysis, we don't expect that a earlier vaccination, during the period considered, neither alters the the number of tests taken nor people mobility, during the same period. We must remark that out treatment is indeed the quicker vaccination program and not the program just by itself. As a consequence, people could anticipate a mass vaccination taking place in the future months and adjust their mobility patterns, but we can assume that they would not travel more because of just being in a country with higher vaccination rate.

Assumption 4 (Non-anticipating potential outcomes) *for all $i \in \{1, \dots, m\}$, the outcome of the unit i at time $t < t_0$ is independent of the treatment that occur in t_0 .*

$$y_{i,t}(\mathbf{w}_{1:m,1:T}) = y_{i,t}(\mathbf{w}_{1:m,1:t_0})$$

This assumption is usually made in the literature (Bojinov and Shephard, 2019; Callaway and Sant'Anna, 2021) to affirm that the future intervention has no influence on pre-intervention statistical units, implying that there is no anticipation of the treatment effect before t_0 . In the empirical application, although the government advertised the forthcoming vaccination campaign, the outcomes, such as the number of deaths, did not shift before the program took place. Furthermore, people had no way to anticipate that the UK program would have been significantly faster compared to other countries.

Assumption 5 (Non-anticipating Treatment) *The assignment mechanism at time t_0 for the unit i depends only on past covariates and past outcomes*

$$p(w_{i,t_0} = \mathbf{w}_{i,t_0} | \mathbf{w}_{1:t_0-1}, \mathbf{y}_{i,1:T}, X_{i,1:T}) = p(w_{i,t_0} = \mathbf{w}_{i,t_0} | \mathbf{y}_{i,1:t_0-1}, X_{i,1:t_0-1})$$

This assumption is the analogous of the *unconfounded assignment mechanism* (Imbens and Rubin, 2015) in a time series framework and ensures that conditionally on past $\mathbf{y}_{i,1:t_0-1}, X_{i,1:t_0-1}$, any variation in the outcomes are to be attributed to the intervention. In our setting, the UK set up a faster vaccination campaign just looking at previous number of deaths and rate of reproduction.

2.3 Causal Estimands

Let $\delta_{i,t} = y_{i,t}(1) - y_{i,t}(0)$ be the individual level (UK) causal effect at time t , then the *additive causal* effect on the subject i at time t is the population average treatment effect and it is given by

$$\tau_{i,t} = \mathbb{E}(\delta_{i,t} | \mathbf{x}_{i,t}).$$

We are also interested in the uncertainty surrounding the treatment effect. This can be either be measured through the variance

$$\varrho_{i,t}^2 = \mathbb{V}(\delta_{i,t} | \mathbf{x}_{i,t}),$$

or directly applying quantile functions to calculate credible regions

$$q_{i,t}^\delta(\alpha) = F_\alpha^{-1}(\delta_{i,t} | \mathbf{x}_{i,t}),$$

with levels of confidence generally set to $\alpha = 95\%$. We aim to estimate these values from a dataset $\mathcal{D} = \{X, y, w\}$, which involves $T = \sum_{i=1}^m T_i$ samples of different time series. The main challenge is that we only observe one of the potential outcomes for every subject i , which implies that the treatment effect is unobserved, so we cannot directly estimate $\tau_{i,t}$.

In addition to its point-wise impact, we are interested in the cumulative effect of the intervention over-time

$$\mathcal{T}_i = \sum_{t=t_0+1}^{T_i} \tau_{i,t} \tag{1}$$

where t_0 represents the time in which the intervention takes place. The cumulative sum is a suitable measure when $y_{i,t}$ is a *flow* variable which is measured over an interval of time (e.g. number of deaths in a country). This quantity however loses its interpretability when $y_{i,t}$ is a *stock* variable, i.e. a quantity measured at a specific time, representing a quantity existing at that point in time (e.g. rate of infectiousness). In this case, it is more meaningful to use the average treatment effect of the intervention

$$\bar{\tau}_i = \frac{1}{T_i - t_0} \sum_{t=t_0+1}^{T_i} \tau_{i,t} = \frac{\mathcal{T}_i}{T_i - t_0} \tag{2}$$

This measure extends Sävje et al. (2019) to the time series framework of the average distributional shift effect since here it is averaged across time as opposed to units.

Within a GP framework, expected values and variances are straightforward to derive and we have that $\delta_{i,t} \sim \mathcal{N}(\tau_{i,t}, \varrho_{i,t}^2)$. Sometimes however, Gaussian likelihoods may not be appropriate and some mathematical transformations may be needed. For example a random variable which takes only non-negative values (e.g. counts, lengths) would be better represented using a log-normal distribution. Thus, if a random variable $\delta_{i,t}^* = \log(\delta_{i,t})$ has a Gaussian distribution, then $\delta_{i,t}^* \sim \log \mathcal{N}(\tau_{i,t}^*, \varrho_{i,t}^{*2})$ is log-normally distributed. By directly modelling the transformed variable one obtains that the causal effect given by

$$\delta_{i,t}^* = \exp(\log y_{i,t}(1) - \log y_{i,t}(0)) = \frac{y_{i,t}(1)}{y_{i,t}(0)}$$

Then, taking the expectation $\mathbb{E}[\delta_{i,t}^* | \mathbf{x}_{i,t}] = \tau_{i,t}^*$ and using the fact that $\delta_{i,t}^*$ is log-normal

$$\tau_{i,t}^* = \mathbb{E}\left(\frac{y_{i,t}(1)}{y_{i,t}(0)} | \mathbf{x}_{i,t}\right) = \exp\left(\tau_{i,t} + \frac{\varrho_{i,t}^2}{2}\right),$$

with related percentiles equations as in 2.3. This can be interpreted as a *multiplicative causal effect* with base 1. A ratio above (resp. below) 1 indicates a positive (resp. negative) effect of the treatment.

Generally for the cumulative effect (1) and average effect (2), there is no closed form solution unless each $\delta_{i,t}$ is normally distributed and independent over time. In this case one can use samples from the posterior predictive distribution over the counterfactual variable to obtain samples from the posterior causal effect distribution, the quantity we are interested in. This method also works when using variable transformations as one can convert it back to the original scale and then calculate the empirical cumulative (average) distribution, with given mean and quantiles.

3 Gaussian Processes

Most of the existing methods in the literature rely on a linear function $f(\cdot)$ in 2. In this paper we aim to relax this linearity assumption and estimate $f(\cdot)$ in a non-parametric fashion, making little assumptions regarding its form. This is achieved using Gaussian Processes (GPs) that generally provide a powerful Bayesian method for regression and classification problems (Rasmussen and Williams, 2006). The function $f(\cdot)$ is treated as an unknown parameter and is assigned a suitable prior distribution defined by a user-specified kernel. Inference and prediction tasks are then carried out based on the corresponding posterior and predictive distribution, which also reflect the uncertainty of the estimation procedure.

3.1 Single Output Gaussian Process

Let $\mathbf{y} = \{y_1, \dots, y_T\} \in \mathbb{R}^T$ the time series of the treated country (the UK) and $X = \{\mathbf{x}'_1, \dots, \mathbf{x}'_T\}' \in \mathbb{R}^{T \times d}$ the matrix of the d associated covariates. Define $Z = \{\mathbf{z}'_1, \dots, \mathbf{z}'_T\}' \in \mathbb{R}^{T \times m-1}$ the matrix containing the time series of the relevant units for the synthetic control (the other European countries). Then $X^* = \{X', Z'\}'$ is the matrix of $d + m - 1$ the time-varying covariates, all with sample size T. A single-output GP (SOGP) takes the form

$$y_t = f(\mathbf{x}_t^*) + \epsilon_t, \quad \epsilon_t \sim \mathcal{N}(0, \omega^2)$$

where ϵ_t is the independent and identically distributed (*i.i.d.*) noise which accounts for the model error. This process is completely defined by its mean $\mu(\mathbf{x}_t^*) = \mathbb{E}[f(\mathbf{x}_t^*)]$ and covariance $k(\mathbf{x}_t^*, \mathbf{x}_s^*) = \mathbb{E}[(f(\mathbf{x}_t^*) - \mu(\mathbf{x}_t^*))(f(\mathbf{x}_s^*) - \mu(\mathbf{x}_s^*))]$ function for each $t, s = 1, \dots, T$. Without loss of generality, we take the mean function to be 0 and consider standard option for the kernel that defines the covariance.

As we will discuss in more details in section 6.1, this approach offers a robust and flexible alternative to Brodersen et al. (2014), but it is also similar in the sense that the \mathbf{x}_t^* 's are not modelled and are assumed to be deterministic inputs. Potential further gains may be achieved if the joint distribution of $(y_t, \mathbf{x}_t^*), \forall t$, is modelled. Such a model is presented in the next section using Multi-output Gaussian processes (MOGP), which generalise GPs in a multivariate framework.

3.2 Multi Output Gaussian Process

MOPGs exploit correlations between multiple outputs and across the input space, thus providing the potential for better predictions, particularly in scenarios with noisy data or missing values (Bonilla et al., 2008). In this paper, we

are going to focus on a class of models referred to as Linear Model of Coregionalization (LMC), in which each output corresponds to a linear combination of one or more latent random functions. These shared processes help transfer the common information across units, without the need to specify a different kernel structure for each output. This is potentially useful in our context, as we want to incorporate knowledge from the other countries without making the model dependent on numerous state-specific parameters. Compared to the SOGP, the MOPG jointly models all the countries, each one with the appropriate set of covariates.

Define $\mathbf{y} = \{\mathbf{y}_1', \dots, \mathbf{y}_m'\}'$, where $\mathbf{y}_i' = \{y_{i,1}, \dots, y_{i,T_i}\} \in \mathbb{R}^{T_i}$ is the time series vector of observed variables and $X = \{X_1', \dots, X_m'\}'$ with $X_i \in \mathbb{R}^{T_i \times d}$ the matrix of the d covariates associated with output i , where i is the country. For the independent variables we assume an *heterotopic data* configuration (Liu et al., 2018), i.e. each output potentially has different time-varying covariates associated with it, $X_1 \neq \dots \neq X_m$ each one with T_i samples such that $T = \sum_{i=1}^m T_i$. In this way, we can model the relationship incurring in each input-output set. The MOPG model is shown below,

$$y_{i,t} = f_{i,t}(\mathbf{x}_{i,t}) + \epsilon_{i,t}, \quad \epsilon_{i,t} \sim \mathcal{N}(0, \omega_i^2),$$

for each $i = 1, \dots, m$ and $t = 1, \dots, T_i$ and where the *i.i.d.* noise $\epsilon_{i,t}$ accounts for the observation errors. The likelihood function for the m outputs is defined as

$$\mathbf{y}|\mathbf{f}(X), X, \Omega \sim \mathcal{N}(\mathbf{f}(X), \Omega),$$

where $\Omega = \text{diag}(\omega_1^2 \mathbf{I}_{T_1}, \dots, \omega_m^2 \mathbf{I}_{T_m}) \in \mathbb{R}^{T \times T}$ and the outputs $\mathbf{f}(X) = \{f_1(X_1), \dots, f_m(X_m)\}'$ are probability distributions in function space and represent the MOPG

$$\mathbf{f}(X) \sim \mathcal{GP}(\mu(X), \mathcal{K}(X, X)).$$

Without loss of generality one can assume that $\mu(X) = \mathbf{0}$ while $\mathcal{K}(X, X) \in \mathbb{R}^{mT \times mT}$ is the multi-output positive semidefinite covariance matrix, defined as

$$\mathcal{K}(X, X) = \begin{bmatrix} K_{1,1}(X_1, X_1) & K_{1,2}(X_1, X_2) & \dots & K_{1,m}(X_1, X_m) \\ K_{2,1}(X_2, X_1) & K_{2,2}(X_2, X_2) & \dots & K_{2,m}(X_2, X_m) \\ \vdots & \vdots & \ddots & \vdots \\ K_{m,1}(X_m, X_1) & K_{m,2}(X_m, X_2) & \dots & K_{m,m}(X_m, X_m) \end{bmatrix}$$

with $K_{i,j}(X_i, X_j) = K_{j,i}(X_j, X_i)'$ $\forall i, j$ by symmetry. Taking a look at block matrices $K_{i,j}(X_i, X_j) \in \mathbb{R}^{T_i \times T_j}$, they are defined such that

$$K_{i,j}(X_i, X_j) = \begin{bmatrix} k(\mathbf{x}_{i,1}, \mathbf{x}_{j,1}) & \dots & k(\mathbf{x}_{i,1}, \mathbf{x}_{j,T_j}) \\ \vdots & \ddots & \vdots \\ k(\mathbf{x}_{i,T_i}, \mathbf{x}_{j,1}) & \dots & k(\mathbf{x}_{i,T_i}, \mathbf{x}_{j,T_j}) \end{bmatrix}, \quad i, j = 1, \dots, m.$$

The next step is to define the kernel for the covariance of each of the GPs $f(\mathbf{x}_j)$. Each kernel depends on a set of hyper-parameters ϕ which determine its structure. For simplicity, let us focus first on the case of $i = j$, so we can drop the unit subscript.

The squared exponential kernel is a popular choice:

$$k_\phi(\mathbf{x}_s, \mathbf{x}_t) = \sigma^2 \exp \left(- \sum_{r=1}^d \frac{(x_{s,r} - x_{t,r})^2}{2\ell_r^2} \right).$$

where r is the r -th input and $\phi = \{\ell_1, \dots, \ell_d, \sigma^2\}'$. From this equation, we can see that the inverse of ℓ_r^2 regulates the how sensitive the kernel covariance is to changes in the r -th dimension of the input. For large values of ℓ_r^2 , the inverse approaches zero, which will cause the value of the covariance to be invariant to the change in $(x_{s,r} - x_{t,r})^2$. This effect will then rule the relevance of the $t - rh$ input to the kernel, hence, the name automatic relevance determination (ARD).

Another useful kernel is the Matérn kernel given by:

$$k_\phi(\mathbf{x}_s, \mathbf{x}_t) = \sigma^2 \frac{2^{1-\nu}}{\Gamma(\nu)} \left(\frac{\sqrt{2\nu}}{\ell} \|\mathbf{x}_s - \mathbf{x}_t\|^2 \right)^\nu J_\nu \left(\frac{\sqrt{2\nu}}{\ell} \|\mathbf{x}_s - \mathbf{x}_t\|^2 \right) \quad (7)$$

with $\phi = \{\ell, \sigma^2\}'$ and where $J_\nu(\cdot)$ is the modified Bessel function and $\Gamma(\cdot)$ is the gamma function. When the dimension $d = 1$ we have that this kernel generates a continuous-time version of an AR(p) Gaussian process where $p = \nu - 1/2$. A particular case is achieved with $\nu = 1/2$, since the Matérn kernel reduces to the exponential kernel given by $k_\phi(\mathbf{x}_s, \mathbf{x}_t) = \exp(-\|\mathbf{x}_s - \mathbf{x}_t\|/\ell)$ which is the covariance process of a Ornstein-Uhlenbeck (OU) process, the continuous-time analogue of an AR(1) process. Let us focus on the one-dimensional case with $\mathbf{x}_t = t$, i.e. the only covariate is time and let us call the lag between two time points Δ . It is shown that taking the Fourier transform of the power spectrum of an OU process on \mathbb{R} with drift ϕ and diffusion σ gives

$$k(\Delta) = \frac{\sigma^2}{2\phi} e^{-\phi|\Delta|} \quad (8)$$

Thus, the exponential decay rate of the autocorrelation is captured using t instead of a lagged version of y_t . Both the above kernels are stationary, i.e. the covariance function depends on the relative positions of two inputs and not their absolute location.² If $k(x_1, x_1)$ and $k(x_2, x_2)$ are covariance functions over different spaces \mathcal{X}_1 and \mathcal{X}_2 , then the direct sum $k(x, x) = k_1(x_1, x_1) + k_2(x_2, x_2)$ and the tensor product $k(x, x) = k_1(x_1, x_1) \cdot k_2(x_2, x_2)$ are also covariance functions (defined on the product space $\mathcal{X}_1 \times \mathcal{X}_2$), by virtue of the sum and product constructions. We can then flexibly sum or multiply all the kernels to have the type of interaction we need in the covariance matrix. As an example a linear kernel plus a periodic one will generate a periodic kernel with a trend.

3.3 Multi Output Kernels

Finally, in order to fully specify the distribution of $\mathbf{f}(X)$, which is a GP with multiple outputs, we need to make an assumption about the dependence between $f_i(\mathbf{x}_i)$'s. The simplest case is to assume independence which will imply the following covariance structure $\mathcal{K} = \text{diag}(K_{1,1}(X_1, X_1), \dots, K_{m,m}(X_m, X_m))$. Alvarez et al. (2012) gives a survey of several more flexible methods including the intrinsic coregionalisation model (ICM), the semiparametric latent factor model (SLFM) and the linear model of coregionalisation (LMC). These models may be viewed as performing exploratory factor analysis on \mathcal{K} with unobserved factors $u_q(X)$. In particular, let us consider the LMC. This specification, widely used in geostatistics, expresses the outputs as a linear combination of Q latent functions as

$$f_i(X_i) = \sum_{q=1}^Q \lambda_{i,q} u_q(X_i)$$

where $u_q(X_i)$ is itself a latent Gaussian process with mean $\mathbf{0}$ and $\text{Cov}[u_q(X_i), u_q(X_i)] = K_q(X_i, X_i)$, while $\lambda_{i,q}$'s are the coefficients which measure output correlations. Furthermore, the model assumes that the latent processes,

²To allow some flexibility in the model, especially when data exhibit visible trends, one can introduce *non-stationary* kernels. The most simple example is the linear kernel. This is defined as $k_\phi(\mathbf{x}_s, \mathbf{x}_t) = \sigma_i^2 \mathbf{x}_s' \mathbf{x}_t$ where $\phi = \sigma^2$

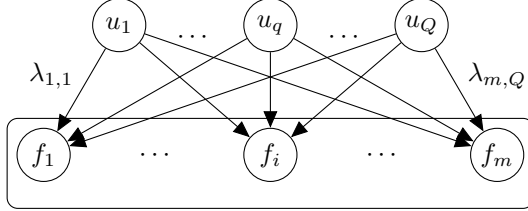


Figure 1: Structure of a LCM. u_q and f_i represent the latent and observed function, respectively. $\lambda_{i,q}$ is the weight associated to each function.

$u_q(X_i)$ and $u_p(X_i)$ for $p \neq q$ are independent and such that $\text{cov}[u_q(X_i), u_p(X_i)] = 0$. Then, cross covariances between the output can be calculated by

$$K_{i,j}(X_i, X_j) = \sum_{q=1}^Q \lambda_{j,q} \lambda_{i,q} K_q(X_i, X_j)$$

Linear combinations of different kernels still result in a valid positive definite covariance matrix. This approach is defined *separable* (Alvarez et al., 2012) due to the decoupled input-output structure of the covariance.

If we define \mathbf{B}_q as the rank 1, $m \times m$ positive semi-definite matrix such that $\mathbf{B}_q = \boldsymbol{\lambda}_q \boldsymbol{\lambda}_q' + \mathbf{k} \mathbf{I}_q$ where $\mathbf{k} = \{k_{1,q}, \dots, k_{q,m}\}$ and $k_{j,q}$ positive and $\boldsymbol{\lambda}_q = \{\lambda_{1,q}, \dots, \lambda_{m,q}\}'$. Then, one can write the multi-output covariance as

$$\mathcal{K}(X, X) = \sum_{q=1}^Q \mathbf{B}_q \otimes K_q(X, X) \quad (9)$$

The coregionalisation matrix \mathbf{B} defines the amount of *inter* and *intra* task transfer of learning among all the outputs. Thus, the latent kernel is shared across all the outputs but is scaled by a factor $\mathbf{B}_q^{[i,j]}$. For example, it is possible that in France, the rate of contagiousness is predicted better by the mobility data than it is in the remaining countries. In this case the \mathbf{B} entry associated with France will be higher compared to other countries.³ Denote by $\bar{X} \in \mathbb{R}^{T \times (d-1)}$ the matrix of d inputs minus *time*, which is denoted by t . Let us consider specifically the time series defined in (6). Using the structure of 9 we will focus on a particular specification given by

$$\mathcal{K} = \mathbf{B}_1 \otimes K_{rbf}(\bar{X}, \bar{X}) + \mathbf{B}_2 \otimes K_{Mat}(t, t), \quad (10)$$

where $K_{rbf}(\cdot)$, $K_{Mat}(\cdot)$ are the squared exponential and Matérn kernels respectively. This combination captures both stationary trends between the output and the input and the autocorrelation structure for each output. Using the time trend as a separate covariate creates a distinctive kernel structure in which it's possible to see how $y_{i,t}$ is related to the other $y_{j,s}$, $\forall i, j, t, s$, something SOGPs cannot do, as shown in the second graph of Figure 4 and 6. If some country i has little to no relation to another country j the terms of $\mathbf{B}_2^{[i,j]}$ will be close to 0.

3.4 SOGP vs MOPG comparison

Although simpler in nature, SOGPs presents some limitations when compared to MOPGs.

First, there is a considerable data loss when applying a univariate approach as opposed to the multivariate *heterotopic*

³The special case of $Q = 1$, generate to the intrinsic coregionalization model (ICM). The computational complexity is largely reduced in exchange of a more restrictive architecture, as one latent process becomes only the source of variability among outputs.

data configuration. We lose all information contained in the covariates of the control countries. Even including them, it won't benefit the model performance because we don't expect for example that the number of deaths in the UK is affected by *mobility data* of any other European country. And still we would face a high dimensional input with potentially more parameter to estimate. Another crucial aspect of the univariate setting is that data is lost because the sample length of the training data is reduced. When we estimate the model we can only use as much data as the minimum sample length of each variable. Both treated and controls are restricted before the intervention⁴. In the multivariate case we narrow the UK dataset up to t_0 but for the other countries we take advantage of the whole dataset. The goal of the multivariate case is to learn the common relationships between input-output, and the more data is fed into the system, the smaller the uncertainty surrounding prediction.

A second important aspect is variable time matching. Most of the studies involving causal estimates related to Covid-19 do not compare countries on a calendar-day basis since the virus hit each country at different dates (see Ghayda et al. (2020) for a meta-study on the comparison between the use of calendar date and days since the outbreak). For example, Born et al. (2020) use a common reference point to initialize observations for each country: $t = 1$ is the day when the number of total positive cases surpasses a threshold of one infection per one million people. This will ensure the effect of the pandemic is comparable across countries. In the MOGP setting, each country is temporally dependent on the others thanks to a separate kernel structure on time. This takes into consideration relative time distance, such as how many days it takes on average to pass from the peak number of deaths to half this number. This information is encoded into the kernel hyperparameters which define a rate of decay such as ϕ in (8). The kernel then links each time point in the treated series to all points in the control time series. This type of architecture is displayed in the third picture of Figure 4 and Figure 6.

Finally, a feature that is related to SOGP when applied to causal analysis is that of input dimensionality. While in the MOGP framework each dependent variable has his own associated covariates, in SOGP the auxiliary outcomes are added to the pool of independent variables X . If the dimensionality of the input space is low, then learning the link function is a much easier problem than learning a high-dimensional function. Though GPs are capable of dealing with large-dimensional covariates in theory, there are several practical and computational issues to consider in its implementation (Tripathy et al., 2016). The inclusion of more input variables (not necessarily related to the response variable) can increase model fit quality, but may lead to poor future predictions due to variance-bias trade off (Cawley and Talbot, 2007). Furthermore, from a computational point of view, optimization becomes more challenging as too many covariates can result in a singular Hessian matrix (Djolonga et al., 2013).

4 Estimation

There are different approaches to GPs parameter and hyperparameters estimation. The Bayesian framework provides effective and consistent inference tools for the former issue. GPs, can indeed be treated as hierarchical models, where the parameters are represented by the latent function $\mathbf{f}(X) = \mathbf{f}$, which in turn can be considered samples from a population characterised by hyper-parameters θ 's. In this case, $\theta = \{\phi', \lambda', \omega^2'\}'$ contain the parameters of the kernel covariance functions ϕ , the components of the corregionalization matrix B , and likelihood variances $\omega^2 = \text{diag}(\Omega)$.

⁴it is still possible to add lagged or forward version of other countries, although this would inevitably impact input dimensionality

Given Bayes rule, the posterior over the parameters is

$$p(\mathbf{f}|\mathbf{y}, X, \boldsymbol{\theta}) = \frac{p(\mathbf{y}|\mathbf{f}, X)p(\mathbf{f}|\boldsymbol{\theta})}{\int p(\mathbf{y}|\mathbf{f}, X)p(\mathbf{f}|\boldsymbol{\theta}) d\mathbf{f}}$$

where $p(\mathbf{y}|\mathbf{f}, X)$ is the *likelihood*, $p(\mathbf{f}|\boldsymbol{\theta})$ is the prior and the expression in the denominator is a normalizing constant, called *marginal likelihood*. We can then express the hyperparameters posterior, making the marginal likelihood from above play the role of the likelihood so that

$$p(\boldsymbol{\theta}|\mathbf{y}, X) = \frac{p(\mathbf{y}|X, \boldsymbol{\theta})p(\boldsymbol{\theta})}{\int p(\mathbf{y}|X, \boldsymbol{\theta})p(\boldsymbol{\theta}) d\boldsymbol{\theta}} \quad (11)$$

The main toolkit for the analysis and optimization is GPy, a Gaussian Process (GP) framework written in Python.⁵

4.1 Type II Maximum Likelihood

In practice, instead of maximizing the posterior in (11), one can instead maximize the marginal likelihood, with respect to the hyperparameters $\boldsymbol{\theta}$ (*Type II Maximum Likelihood*)

$$p(\mathbf{y}|X, \boldsymbol{\theta}) = \int p(\mathbf{y}|\mathbf{f}, X, \boldsymbol{\theta})p(\mathbf{f}|X, \boldsymbol{\theta}) d\mathbf{f}$$

The strength of GPs is the tractability of the integral over the parameters \mathbf{f} , since we know that $p(\mathbf{f}|X, \boldsymbol{\theta}) = \mathcal{N}(\mathbf{f}|0, \mathcal{K})$. Furthermore, we have that $p(\mathbf{y}|\mathbf{f}, \boldsymbol{\theta}) = \mathcal{N}(\mathbf{y}|\mathbf{f}, \Omega)$. Then, following Rasmussen and Williams (2006), one can perform the integration of the product of two normals which yield the log marginal likelihood

$$\log p(\mathbf{y}|X, \boldsymbol{\theta}) = -\frac{1}{2}\mathbf{y}'\Sigma\mathbf{y} - \frac{1}{2}\log|\Sigma| - \frac{T}{2}\log(2\pi), \quad (12)$$

where $\Sigma = \mathcal{K} + \Omega$ is the covariance matrix of the noisy outcome \mathbf{y} and contains all *hyper-parameters*. The first term is a data-fit term, as it is the only one involving y , the second one represents the complexity term, since it depends only on the covariance function, and the last one is a constant. Marginalising out the Gaussian vector \mathbf{f} , moves up the Bayesian hierarchy by one level, thus reducing the odds of overfitting (Murphy, 2013). To maximize the marginal likelihood we first find the derivative of the marginal likelihood with respect to the kernel hyperparameters

$$\frac{\partial}{\partial\theta_i} \log p(\mathbf{y}|X, \boldsymbol{\theta}) = \frac{1}{2}\mathbf{y}'\Sigma^{-1}\frac{\partial\Sigma}{\partial\theta_i}\Sigma^{-1}\mathbf{y}' - \frac{1}{2}\text{tr}\left(\Sigma^{-1}\frac{\partial\Sigma}{\partial\theta_i}\right),$$

where $\frac{\partial\Sigma}{\partial\theta_i}$ depends on the structure of the kernel and the parameters we are taking derivatives of. The inversion of the \mathcal{K} matrix requires $\mathcal{O}(n^3)$ by standard methods, and then $\mathcal{O}(n^2)$ time per hyperparameter to calculate the gradient. Given the minor relative computational cost of calculating derivatives, a gradient based optimizer would be beneficial.⁶ A very popular method is BFGS, named after its inventors Broyden, Fletcher, Goldfarb and Shanno (Fletcher, 2000). As a Quasi-Newton procedure it approximates the Hessian using the differences of gradients over several iterations, thanks to a *secant* (Quasi-Newton) condition.

⁵<https://sheffieldml.github.io/GPy/>. Following the authors proposal, we will treat the *nugget* parameters \mathbf{k} as a parameter to optimize in order to increase numerical stability. These parameters are in the parametrization of $\mathbf{B}_q = \boldsymbol{\lambda}_q\boldsymbol{\lambda}_q' + \mathbf{k}\mathbf{I}_q$ to guarantee the positive definiteness of the kernel.

⁶Generally, the objective function is non-convex and local minima exist and can make the optimization procedure challenging. However, empirical studies with non-complex covariance functions seem to indicate that the issue is not extremely serious, as every local maxima correspond to a different interpretation of the data (Rasmussen and Williams, 2006)

Algorithm 1 BFGS method

```

1: choose initial guess  $\theta_0$ 
2: choose  $B_0$ , the initial Hessian guess, e.g.  $B_0 = \mathbf{I}$ 
3: for  $k = 0, 1, 2, \dots$  do
4:   solve  $B_k \mathbf{s}_k = -\nabla f(\theta_k)$ 
5:    $\theta_{k+1} = \theta_k + \mathbf{s}_k$ 
6:    $\mathbf{y}_k = \nabla f(\theta_{k+1}) - \nabla f(\theta_k)$ 
7:    $B_{k+1}^{-1} = B_k + \frac{\mathbf{y}_k \mathbf{y}_k'}{\mathbf{y}_k' \mathbf{s}_k} - \frac{B_k \mathbf{s}_k \mathbf{s}_k' B_k}{\mathbf{s}_k' B_k \mathbf{s}_k}$ 
8: end for

```

The standard BFGS method employs the full history of gradients to calculate the Hessian approximation. The limited memory BFGS, abbreviated as L-BFGS, uses only the most recent (usually 20) gradients to compute the product $B_k^{-1} \nabla f(\theta_k)$. The main advantage of L-BFGS is that it requires less storage than $n(n + 1)/2$ elements required to store the Hessian estimate, requiring only $\mathcal{O}(sn)$ instead of $\mathcal{O}(n^2)$ (Nocedal and Wright, 2006).

The L-BFGS-B algorithm further extends L-BFGS to handle linear constraints on variables such that $l_i \leq \theta_i \leq u_i$ where l_i and u_i are constant lower and upper bounds for each θ_i . The algorithm separates fixed and unconstrained variables at each step by using the gradient method. Subsequently, it employs the L-BFGS method on the free variables to achieve higher accuracy.

4.2 Hamiltonian Monte Carlo

The most popular Bayesian methods rely on MCMC, which can be quite slow for a high dimensional parameter space. It is possible to approximate the posterior over the latent functions and over the hyper-parameters after setting the priors, using Hamiltonian Monte Carlo (HMC). Here, an additional *momentum* variable $\phi \sim \mathcal{N}(\mathbf{0}, \mathbf{M})$ is introduced for each parameter θ , which is regarded as *position*. The covariance matrix \mathbf{M} , called the mass matrix, rotates and scales the target distribution and it is generally set to the identity matrix, $\mathbf{M} = \mathbf{I}$, when no information is available on the target distribution. The joint density $p(\phi, \theta)$ defines the Hamiltonian

$$\begin{aligned}
H(\phi, \theta) &= -\log p(\phi, \theta) \\
&= -\log p(\phi|\theta) - \log p(\theta) \\
&= T(\phi|\theta) + V(\theta).
\end{aligned}$$

The first term $T(\phi|\theta) = -\log p(\phi|\theta)$ is called *kinetic energy* and it is equal to the squared of the momentum since $-\log p(\phi|\theta) = \log p(\phi) = 0.5\phi' \phi$, being the momentum density independent of the target density. The second term $V(\theta) = -\log p(\theta)$ is the *potential energy* and is related to the target distribution $p(\theta)$. This extended model then follows Hamiltonian dynamics through fictitious time, whose evolution depend on a set of differential equations:

$$\begin{aligned}
\frac{d\theta}{dt} &= +\frac{\partial H}{\partial \phi} = \frac{\partial T}{\partial \phi} \\
\frac{d\phi}{dt} &= -\frac{\partial H}{\partial \theta} = -\frac{\partial T}{\partial \theta} - \frac{\partial V}{\partial \theta} = -\frac{\partial V}{\partial \theta},
\end{aligned}$$

since $\frac{\partial T}{\partial \theta} = 0$ by independence. The solution to these differential equation is not available in closed form and must be computed numerically. The most popular numerical integrator, which preserves volume and reversibility of the system is the *Leapfrog* integrator (Girolami and Calderhead, 2011). The leapfrog integrator takes L steps, each one of size ϵ and iterates between a half step for the momentum and a full-step update for the position.

$$\begin{aligned}\phi_{t+\frac{\epsilon}{2}} &= \phi_t - \frac{\epsilon}{2} \frac{\partial V}{\partial \theta_t} \\ \theta_{t+\epsilon} &= \theta_t - \epsilon M^{-1} \phi_{t+\frac{\epsilon}{2}} \\ \phi_{t+\epsilon} &= \phi_{t+\frac{\epsilon}{2}} - \frac{\epsilon}{2} \frac{\partial V}{\partial \theta_{t+\epsilon}}.\end{aligned}$$

The leapfrog discretisation introduces small numerical errors in the total energy calculation. The correction takes the form of a Metropolis-Hastings step, in which the probability of accepting a proposal (ϕ^*, θ^*) generated from (ϕ, θ) is $\min(1, \exp(H(\phi, \theta) - H(\phi^*, \theta^*)))$. In case of rejection, the previous values are used to initialise the new iterations. In practice, when using HMC two main parameters need to be tuned. Firstly, one needs to chose the appropriate step size. Taking a look to the acceptance rate, it is possible to reduce or increase the value of ϵ . Smaller steps are more computationally expensive but precision may improve. However, a very small ϵ makes it difficult to efficiently explore the target distribution. The best way to determine the appropriate length L of the simulation is to look at the parameters' auto-covariance function, increasing L to achieve more independent samples. Excessively long trajectories can erode computational effort, as the simulation exercise may generate loops, making the destination point the same as the initial one. Once reasonable values for ϵ and L have been determined, desired sample from the target distribution can be obtained.

Generally, for MOPG, the parameter of interest are the λ composing the corregional matrix B which defines the relationships among the outcomes⁷. The conditional posterior of λ can be computed as

$$p(\lambda | \phi, \omega^2, y, X) = \frac{p(y | X, \lambda, \phi, \omega^2) p(\lambda | \phi, \omega^2)}{p(y | X, \phi, \omega^2)}. \quad (21)$$

By maximizing the the denominator in (21) it is possible to obtain the maximum likelihood type II estimates,

$$\{\phi^*, \omega^{2*}\} = \arg \max_{\phi, \omega^2} p(y | X, \phi, \omega^2).$$

Then, the marginal posterior of λ can be approximated by conditioning on the estimates obtained by ML-II optimization as in 12

$$p(\lambda | X, y) = \int p(\lambda, \phi, \omega^2 | X, y) d\phi d\omega^2 \approx p(\lambda | X, y, \phi^*, \omega^{2*})$$

In this way one can focus the attention and computational burden only on the parameter of interest. As a robustness check, we will try to free up ω^2 as well, in order to account for the estimation uncertainty coming from the observational errors. The algorithm is performed using *GPy* and employing 5000 samples, an identity mass matrix $M = I$ and starting values of $\epsilon = 0.01$

4.3 Prior Specification

In order to adopt a Bayesian approach to inference, we need to specify a prior distribution $p(\theta)$. We select a *weakly informative* prior distribution (Gelman et al., 2004), which incorporates enough information to regularise the posterior

⁷In the Bayesian estimation approach we will keep the parameters k fixed.

distribution. In this way we keep the posterior within reasonable values without contributing actively to the knowledge of the underlying parameters. For the loadings, we employ a normal distribution,

$$\lambda_i \sim \mathcal{N}(\mu_\lambda, \sigma_\lambda^2),$$

where \mathcal{N} is the normal distribution with mean μ_λ and variance σ_λ^2 . This former parameter expresses our expectation about the value of each element composing the corregional matrix. In practice, we set $\mu_\lambda = 0$ and $\sigma_\lambda = 10$. Furthermore, we want to specify the set of variance parameters that govern the observational errors. A typical prior distribution for such a variance is

$$\omega_i^2 \sim \mathcal{G}(a, b),$$

with \mathcal{G} being the Gamma distribution with parameters a, b . Those parameters generally depends on our prior belief about the precision surrounding the collection of data. As a default, we set up $a = 0.1$ and $b = 1$. Overall, these specifications provide a useful, although wide default while preserving flexibility in case a more specific prior information is available.

4.4 Posterior Predictive and Causal Estimates

Let us say we want to use observed data \mathbf{x} to make predictions about data $\tilde{\mathbf{x}}$. For example, as we will see in our application, if \mathbf{x} are training data and $\tilde{\mathbf{x}}$ test data. GPs are stochastic processes in which any finite subset of random variables follows a joint normal distribution. Thus, it is possible to determine the joint prior distribution of the observations \mathbf{y} and the output $\tilde{\mathbf{y}} = \mathbf{f}(\tilde{\mathbf{X}})$ at test points $\tilde{\mathbf{X}}$ as

$$\begin{bmatrix} \mathbf{y} \\ \tilde{\mathbf{y}} \end{bmatrix} \sim \mathcal{N} \left[\begin{pmatrix} \mathbf{0} \\ \mathbf{0} \end{pmatrix}, \begin{pmatrix} \mathcal{K}(X, X) + \Omega & \mathcal{K}(X, \tilde{X}) \\ \mathcal{K}(\tilde{X}, X) & \mathcal{K}(\tilde{X}, \tilde{X}) \end{pmatrix} \right]$$

where $\mathcal{K}(X, \tilde{X}) \in \mathbb{R}^{T \times \tilde{T}}$ is the matrix of the covariances calculated at all pairs of training and test points, X and \tilde{X} , respectively. Then it is possible to analytically derive the posterior distribution of $\tilde{\mathbf{y}}$, conditioned on \mathbf{y} , by using multivariate Gaussian proprieties.

$$\tilde{\mathbf{y}} | \mathbf{y}, X, \tilde{X} \sim \mathcal{N}(\tilde{\boldsymbol{\mu}}, \tilde{\boldsymbol{\Sigma}}) \quad (24)$$

where $\tilde{\boldsymbol{\mu}}$ and $\tilde{\boldsymbol{\Sigma}}$ are the predictive mean and predictive variance, given by

$$\begin{aligned} \tilde{\boldsymbol{\mu}} &= \mathcal{K}(\tilde{X}, X)[\mathcal{K}(X, X) + \Omega]^{-1}\mathbf{y} \\ \tilde{\boldsymbol{\Sigma}} &= \mathcal{K}(\tilde{X}, \tilde{X}) - \mathcal{K}(\tilde{X}, X)[\mathcal{K}(X, X) + \Omega]^{-1}\mathcal{K}(X, \tilde{X}) \end{aligned}$$

Thus, the predictive uncertainty $\tilde{\boldsymbol{\Sigma}}$, does not depend on \mathbf{y} , but only on the output dependencies given by the kernel structure of X and \tilde{X} . However, when parameter uncertainty is accounted for, the distribution is no longer Normal as indicated in (24). Given the posterior distributions of the hyperparameters of the model $\boldsymbol{\theta}$ and the function \mathbf{f} , we can calculate the in-sample posterior predictive as

$$p(\tilde{\mathbf{y}} | \tilde{\mathbf{x}}, X, \mathbf{y}) = \int p(\tilde{\mathbf{y}} | \tilde{\mathbf{x}}, \mathbf{f}, \boldsymbol{\theta})p(\mathbf{f} | X, \mathbf{y}, \boldsymbol{\theta})p(\boldsymbol{\theta} | X, \mathbf{y})d\mathbf{f}d\boldsymbol{\theta}. \quad (27)$$

For inference we first simulate draws from the posterior of the hyperparameters, then we simulate GPs for the given set of hyperparameters to obtain prediction samples.

In causal impact analysis we are mainly concerned with the posterior predictive of the counterfactual time series i in the absence of an intervention. To do so we need the out-of-sample forecasts from the distribution

$$p(\tilde{y}_{i,t_0+h} | \tilde{\mathbf{x}}_{i,t_0+h}, X_{i,1:t_0}, \mathbf{y}_{i,1:t_0}, \{X_{j \neq i, 1:T_j}\}, \{\mathbf{y}_{j \neq i, 1:T_j}\})$$

for $h > 0$ and $j = 1, \dots, m$. This is a special case of (27), only with \mathbf{y}_i and X_i restricted for $t < t_0$. Then, we can obtain the counterfactual time series $\tilde{\mathbf{y}}_i^{[k]}(0) = \{\tilde{y}_{i,t_0+1}^{[k]}(0), \dots, \tilde{y}_{i,T_i}^{[k]}(0)\}'$, for $k = 1, \dots, N$ samples. If Assumption 1 through Assumption 5 hold, these values are the realization of $y_{i,t}(0)$ defined in Section 2.3, i.e. the response that would have been observed after the intervention, had the intervention not taken place. It is worth noting that the posterior predictive density is conditional on the observed data of the treated country before the intervention as well as the data in all control countries both before and during the intervention. This is because we assumed temporal no-interference in Assumption 2, stating that the outcome of unit i at a time $t_0 + h$ depends solely on its own treatment path. Furthermore, through Bayesian model averaging, we integrate out all parameters (functions) and hyperparameters, so that the distribution does not depend on particular choice of parameter estimates.

Finally, using the samples $\tilde{y}_{i,t}^{[k]}(0)$, for $k = 1, \dots, N$, it is possible to compute the posterior distribution of the pointwise impact

$$\tilde{\delta}_{i,t}^{[k]} = y_{i,t}(1) - \tilde{y}_{i,t}^{[k]}(0) \quad t = t_0 + 1, \dots, T_i,$$

where $y_{i,t}(1)$ is the observed outcome. As in Brodersen et al. (2014), the density in (27) is a joint distribution over all counterfactual data points, rather than a set of univariate predictive distributions. This ensures that we can correctly estimate the trajectory of the counterfactuals through the dynamic structure defined by the model. The samples are also employed to compute the cumulative and average impact (1) and (2).

5 Empirical Analysis

5.1 Covid-19 Vaccination program

Evidence suggests that vaccination against Covid-19 reduces the risk of severe complications, including death, and slows down the transmission of infections (see Zheng et al. (2022) for a meta-analysis of numerous Covid-19 studies). We are still to determine how much of the observed slow down in the spread and how many lives saved are attributable to fast and effective inoculation policies such as those introduced by the UK, as opposed to more conservative programs, such as the ones implemented for instance in France, Portugal and Greece. The United Kingdom has delivered one of the world's fastest vaccination campaigns, giving the first shot to about 67% of the adult population and a second to 50% by the end of June 2021, potentially helping to reduce deaths and infection rates.⁸ In this application we seek to answer the question above (about impact of quick program) by comparing the observed deaths and reproduction rate in the UK to a "counterfactual UK", a synthetic control constructed using EU countries with less ambitious inoculation programs.

5.2 Data

Our data consists of weekly data points for different countries from 1st March 2020 to 30th June 2021. The date of the intervention t_0 is set to be the 31th January 2021, since that is the first week in which the number of people that

⁸<https://coronavirus.data.gov.uk/details/vaccinations>

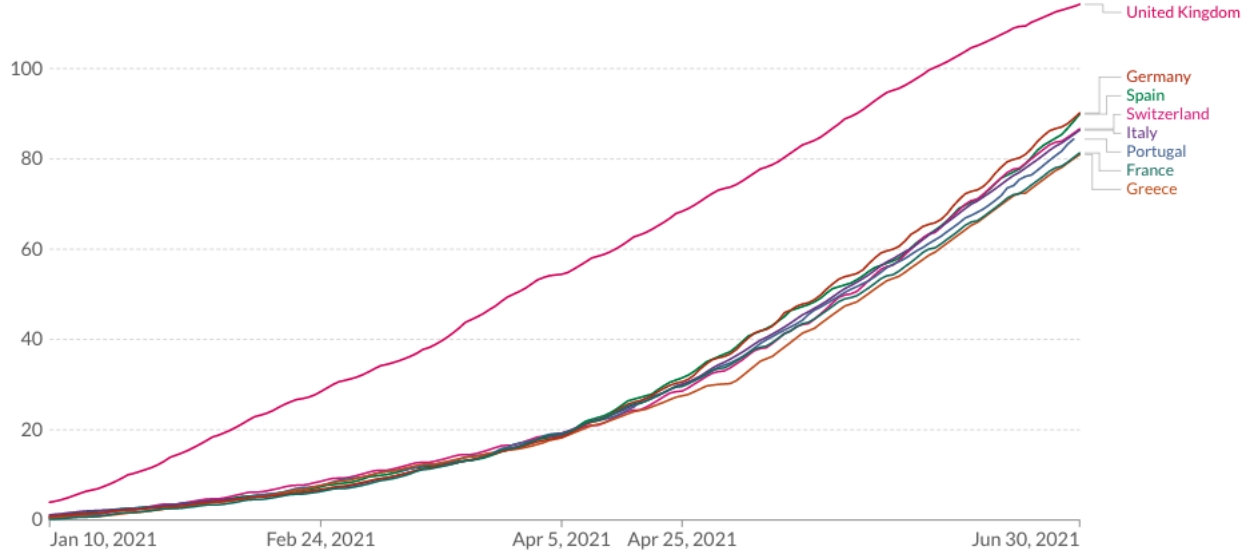


Figure 2: COVID-19 vaccine doses administered per 100 people. Total number of doses administered, divided by the total population of the country. All doses, including boosters, are counted individually. Source: Our World in Data

had the second dose surpassed 500,000. As mentioned above, the treated country for this study is the United Kingdom as its policy differed from that of the other European countries.

We are going to focus our analysis on two different outcome (dependent) variables. The first one is the confirmed Covid-19 deaths per million people. The variable is divided by the population for each country to obtain a continuous variable and then it is converted on a log scale to better handle the asymmetry of the data arising from the absence of negative values. The second variable of interest is the estimate of the reproduction rate (R) of Covid-19. R measures the level of contagiousness of the virus and equals the expected number of cases directly generated by one case in a population where all individuals are susceptible to infection.

To respect the Covariates-treatment independence (Assumption 4), all covariates are considered unrelated to the intervention. They are: i) time trend, ii) Google Mobility Data and, iii) weekly number of Covid-19 tests. The first one is a variable that represent time with $t = 1$ being the first time we have an observation. Since we are working with heterotopic data, each of the outcome variables is associated with different covariates, all with potentially different start times. For example in the *number of deaths* study we have that Italy (the country whose reports are the earliest) first reported on ‘2020-03-15’, thus this time value will be assigned as $t = 1$. The UK first reported on ‘2020-04-19’ and this will be assigned a value $t = 5$, as this date is 5 weeks after $t = 1$. Although the time trend is linearly increasing, the relationship with the dependent variable is not necessarily linear thanks to the flexible structure of the kernel function on the input space. *Google Mobility Report* is a publicly available dataset that records how visits to different places changed overtime, compared to a baseline. The venues covered by the dataset are: grocery and pharmacy, parks, transit stations, retail, recreation, residential and workplaces. Similarly to Her et al. (2022); Chatzilena et al. (2022) we reduce the dimension of the input space performing Principal Component Analysis (PCA) on each country and we use the first principal component as a single variable which represents country mobility. On average more than 80% of the variability of the dataset is explained by this factor, meaning we can ignore other components. The last variable is the weekly average Covid-19 tests per 1000 people.

5.3 Methodology

We now explain the methodology we employ to estimate the causal effects set out in section 2.3. Our main concern is to ensure that the definitive model works well on the observed data before we apply it to creating the counterfactual. To assess the ability of each models to explain the data, we adopt a typical machine learning approach splitting the data into train and test samples. In particular, we only use data from the period before the intervention as we want to avoid having data after the intervention as test samples. Evaluating the models based on data y that are contaminated by the intervention can be viewed as trying to minimise the distance between $y_{i,t}(1)$ and $y_{i,t}(0)$, thus introducing a downward bias on the causal impact estimate. The new dataset is split at time $t^* < t_0$ into two parts, the train and the test set, which account for 2/3 and 1/3 of data, respectively. There are two main issues to address: which countries to choose as control series and which type of kernel structure the model should have.

The first problem involves finding the combination of countries that achieve better predictive performance. Employing a too high number of countries in one model would increase exponentially the number of parameter to estimate. This leads to a greater model complexity, which would make the model prone to over-fitting. As a first step, we perform an early screening on the set by using Dynamic time warping, or DTW (Giorgino, 2009). The algorithm produces a distance metric between two input time series. The similarity or dissimilarity of two time-series is then calculated by converting the data into vectors and calculating the Euclidean distance between those points in vector space. Then, the 8 components which minimise the distance are chosen to be the set of potential control series of the experiment. This algorithm is particularly useful for dealing with sequences in which single components have characteristics that vary over time, not necessarily in sync.

The second issue is related to the appropriate choice of the Intrinsic coregionalization model (ICM) architecture and relevant kernel function. We compare different methods.

- 1) *Two Factor GP* (2FGP). This is the model outlined in the section 3.2 equation (10), in which the rbf kernel is adopted on the input space given by the spatial covariates and the Matérn Kernel on the time trend. This is to say that there are two unobserved and independent latent factors, one given by time, whose covariance structure resemble the continuous-time AR(p) process as outlined in section 3.2, and one given by the non-linear relationship that occurs between the outcome and the covariates. Number of parameters: 31.
- 2) *Independent GPs* (INGP). While the coregionalized model shares information across outputs, the independent models cannot do that. In particular we assume that in (9), $\lambda_q = \mathbf{0}$ and $k_{j,q} = 1 \forall j, q$, i.e. $\mathbf{B}_q = \mathbf{I}_m$. In the regions where there is no training data specific to an output the independent models tend to revert to the prior assumptions. We want to test if there is transfer of learning among all the outputs. Number of parameters: 11
- 3) *One Factor GP* (1FGP). Instead of assuming two separate input spaces and kernels for time and the other covariates as in (9), we combine the two kernels such that $\mathcal{K} = \mathbf{B}_1 \otimes (K_{rbf}(X, X) + K_{Mat}(X, X))$. In this way we combine features of the *rbf* and *Matérn* kernels on a shared input space. This structure implies an unobserved factor common to all tasks, which does not differentiate between time and the other components. However, the model is simpler as require less parameters to estimate. Number of parameters: 21.
- 4) *Two RBF Factor GP* (2RBF). The input space is divided into time trend and spatial covariates but the kernel function has the same structure (Radial Basis Function) for both t and \bar{X} . $\mathcal{K} = \mathbf{B}_1 \otimes K_{rbf}(\bar{X}, \bar{X}) + \mathbf{B}_2 \otimes$

$K_{rbf}(t, t)$. This model test if the rbf kernel structure can better describe time trends as opposed to the *Matérn* kernel. Number of parameters 31.

- 5) *Single Output Gaussian Process* (SOGP). The model referenced in (5), in which the outcome variable is $\mathbf{y} = \mathbf{y}_i$ and the covariates are $\tilde{X} = (\{\mathbf{y}_j\}_{j \neq i}, X_i)$, i.e. all the other control variables and the relevant covariates for the treated subject i . We adopt a single RBF Kernel on the whole input space without ARD to define the covariance structure. Number of parameters: 3
- 6) *Bayesian Causal Impact* (BCI). The *local linear trend* outlined by Brodersen et al. (2014), with the same data structure employed by SOGP. The optimization is performed by using Kalman Filters and MCMC. In both the univariate cases we adopt an *isotopic data* framework.⁹ Number of parameters: 9.

Models 1) to 4) fall into the MOPGs framework defined in Section 3.2, model 5 is the SOGP of section 3, while 6) is a replica of the work of Brodersen et al. (2014). Once the models have been fitted on the training dataset we can evaluate the forecast performance calculating the distance from the observed values. We use different measure of dispersion:

- 1) *Mean Squared Error* (MSE). It computes the average of the squared errors, calculated as the differences between the estimated values and the actual values

$$\text{MSE}_i = \frac{1}{t_0 - t^*} \sum_{t=t^*}^{t_0} (y_{i,t} - \tilde{\mu}_{i,t})^2.$$

where $\tilde{\mu}_{i,t}$ is defined in (26). While simple, the MSE disregards the uncertainty of the predictions..

- 2) *Log Score* (LogS). Forecasts are usually surrounded by uncertainty, and being able to quantify it is pivotal to good decision making. Consider the GP framework of 4.4, with the hyperparameters given by Type II MLE. The logarithmic score (Good, 1952) is defined as

$$\text{LogS}_i = -\frac{1}{t_0 - t^*} \sum_{t=t^*}^{t_0} \log \mathcal{N}(\tilde{\mu}_{i,t}, \tilde{\sigma}_{i,t})$$

where $\tilde{\sigma}_{i,t}$ is the i^{th} diagonal element of $\tilde{\Sigma}$ as in (26). Thus, the score is equal to the log of the predictive density of \mathbf{y}_i given by (24). The measure also takes into consideration the variability of the point forecast. Since we are working with GP the distribution is Normal and available in closed form, making the calculation straightforward. ¹⁰

- 3) *Energy Score* (ES). This scoring rule is the multivariate extension of the the continuous ranked probability score, CRSP (Matheson and Winkler, 1976). Let $\mathbf{y} = \{y_{t^*}, \dots, y_{t_0}\}' \in \mathbb{R}^h$ the values of the outcome i on the h -horizon test set where $h = t_0 - t^*$. Denote by $\tilde{\mathbf{y}}$ the forecast distribution (24) on \mathbb{R}^h with N samples $\{\tilde{\mathbf{y}}^{[1]}, \dots, \tilde{\mathbf{y}}^{[N]}\}$ with $\tilde{\mathbf{y}}^{[k]} = \{\tilde{y}_{t^*}^{[k]}, \dots, \tilde{y}_{t_0}^{[k]}\}$ with $k = 1, \dots, N$, Then, the energy score can be calculated as

$$\text{ES}_i = \frac{1}{N} \sum_{k=1}^N \|\mathbf{y}^{[k]} - \mathbf{y}\| - \frac{1}{2N^2} \sum_{k=1}^N \sum_{c=1}^N \|\mathbf{y}^{[k]} - \mathbf{y}^{[c]}\|$$

⁹For the SOGP and Bayesian Model of (Brodersen et al., 2014) one can use only the number of point such that $T_i = \min(T_1, \dots, T_m)$ while for the Gaussian Process we have heterotopic data in which T_i may be different from T_j .

¹⁰The Gaussian distribution assumption does not hold in general, especially when parameter uncertainty is accounted for. In case of bayesian estimation such as in 4.2 the predictive distribution is no longer Normal. Nonetheless, it is still possible to use the samples obtained from the HMC distribution to calculate the score (Jordan et al., 2019).

where $\|\cdot\|$ is the Euclidean norm on \mathbb{R}^h and $c = 1, \dots, N$. This function evaluates samples from a multivariate forecast and returns a single estimate.¹¹

For a given model, the lower the score, the higher the accuracy of the forecast. All three measures are compared to see which model performs better. At this stage, given the high number of models to fit we perform type II ML to optimize hyperparameters. Bayesian estimation is employed subsequently on the whole dataset to have a more exhaustive estimate of the *causal estimands*.

Before proceeding with the results, we sum up the procedure involved to get to the causal estimands.

- 1) We remove any European country which has no input or output data reported for the period under consideration, i.e from ‘01-01-2020’ to ‘01-06-2021’.
- 2) We restrict the data before the intervention $t \leq t_0$ and split into train $t = 1, \dots, t^* - 1$ and test $t = t^*, \dots, t_0$ set.
- 3) We apply DTW on that period to restrict the number of available countries to 8.
- 4) For any given combination of 4 countries (plus the UK), we train the 6 models outlined in 5.3 and calculate the dispersion metrics. We have 70 combination of countries, for a total of 420 models.
- 5) The combination which results in a lower Energy Score overall, is selected as the best model.
- 6) We fit the selected model on the whole dataset, restricting only the UK before intervention date and calculate optimal θ , through type II ML.
- 7) We perform HMC with 5000 samples on the parameters λ that define the correlation matrix B, leaving the others fixed to their MLE values.
- 8) Given the obtained samples of hyperparameters, we calculate the prediction distributions and related causal estimands.

The steps 1) to 5) take place before the intervention t_0 while 6) to 8) deal with the post-intervention analysis. The latter study is applied first to the weekly deaths per million people data and subsequently for the weekly infection rate R.

6 Results

6.1 Before Intervention: Model Comparison

We start by applying the DTW algorithm to select the countries that are most similar to the UK. This process restricts the pool of European candidates for each outcome. Given these countries we focus on forecasting performance before the intervention t_0 to assess the performance of the various models. We fit the ones in 5.3 for each country combination and select those that achieve the lowest possible Energy Score. Taking a look at Table 1, we see that the 2FGP achieves the lowest Energy Score for both of the analyses. The other two GP-based models (1FGP and 2RBF) perform well overall but slightly worse compared to the base model (2FGP). The INGP is the worse GP model since it cannot rely

¹¹Sampling from the forecast distribution can be regarded as an approximation the values of the proper scoring rules, for a sufficient large N (Jordan et al., 2019).

	Weekly deaths per million people					
	2FGP	1FGP	2RBF	INGP	SOGP	BCI
MSE	0.8189	0.8274	1.2754	4.2811	0.7263	3.1693
logS	0.2389	0.4624	0.3451	1.1465	0.4008	4.7445
ES	0.6776	0.7791	0.8820	2.7745	0.7025	2.6261

	Weekly infection rate R					
	2FGP	1FGP	2RBF	INGP	SOGP	BCI
MSE	0.3597	0.4679	0.4028	2.1470	0.4905	0.5386
logS	-0.6960	-0.6815	-0.8182	0.7835	-0.6173	-0.5928
ES	0.2883	0.3354	0.2915	1.4496	0.3505	0.3794

Table 1: Comparison of the different measures of prediction error outlined in 5.3 according to different models. Lowest values, which indicate good predictive performances are indicated in bold

on the part of data after the training threshold $t > t^*$, thus converging to the dependent variable average values. The SOGP performance is solid on the Weekly Deaths application and on the infection rate. Although the dataset used is the same as BCI, the latter model employs a state-space framework in which the time layout is given by a random walk. Thus in the case of the SOGP outperforming the BCI, it means that the non-linearity of variables provides a better ground for model prediction than modelling the time dynamics through a linear equation. Nonetheless, the two univariate models produce comparable trajectories, but in general BCI tends to underestimate the uncertainty, resulting in a lower Energy Score¹². As mentioned above, MOPGs still possess a time structure without sacrificing non-linearity. Another comparison of the model performance is displayed in Figure 3, where each model is represented by a different coloured line, and the crosses serve as the observations.

6.2 After Intervention: Causal Effect

6.2.1 Weekly deaths per million people

Once the model and the countries are established, it is possible to fit the model to the whole data set, restricting only the UK in the period before intervention. For the analysis where the outcome is weekly deaths per million, the best results are achieved using five countries, namely ‘Italy’, ‘Netherlands’, ‘Ireland’, ‘Portugal’. Using type II Maximum likelihood as in (12) one can obtain the optimal hyperparameters for the kernels. The estimated kernel matrices are of dimension $mT \times mT$ where $T = \sum_{i=1}^m T_i$ and represent the variances and covariances of each data point. Understanding the kernel function of a GP is essential to interpreting the association not only between variables but also among different data points belonging to different variables. The kernel on the left of Figure 4 is \mathcal{K} , which is the sum of the outer products of each kernel times the coregionalization matrix B . Each of the m blocks represent the variance-covariance matrix of each process $f_j(\mathbf{x}_j)$. The upper left block is the one corresponding to the UK and it is smaller compared to the others, as only pre-intervention data is included. A first visual inspection of \mathcal{K} , shows

¹²Overall scores are far worse including a linear trend as a covariate in the SOGP, so we decided to drop it.

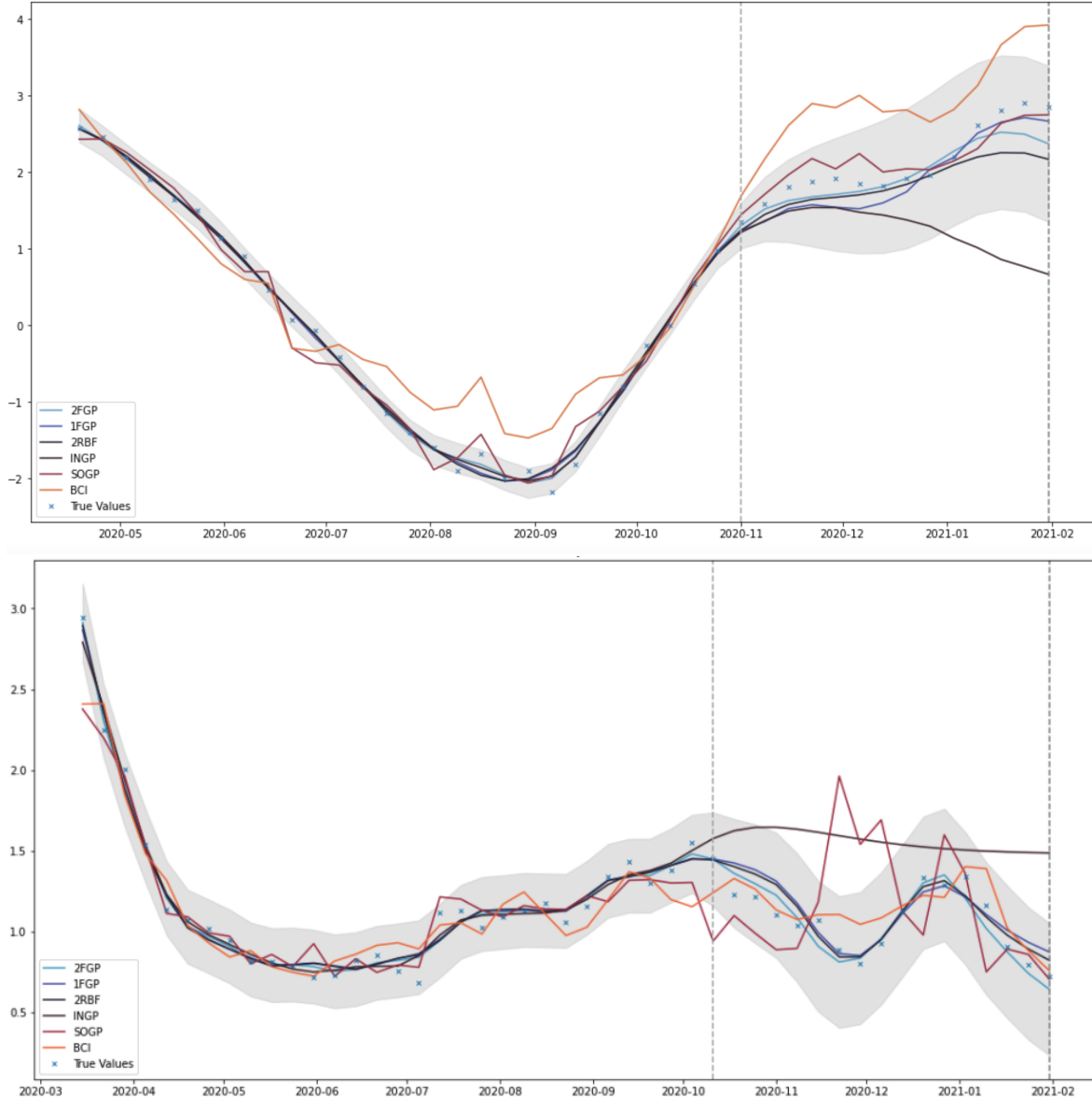


Figure 3: Top: Predicted log weekly deaths per 1000 people for the different models. Bottom: Predicted rate of infectiousness for the different models. The blue crosses represent observed data, and each line correspond to a specific model. The first vertical gray dotted line separates t^* which divide between the train and test dataset. The second vertical dashed line identifies t_0 . The gray shaded area represents 95% prediction interval of the 2FGP, the base model.

that the time component accounts for the majority of the variability as values range from 0 to 2. Furthermore, we see that *mobility data* and *number of tests* were very important variables to explain Ireland (fourth country) but almost not influential in the Netherlands (third country). However, we see how the independent variables of other countries explain very little for the UK (top row/column of the matrix). The time-domain coregionalization matrix is more homogeneous and we can see that UK weekly death followed a pattern more similar to Ireland as we observe slightly higher values of $B_{2,[2,4]}$ compared to other countries. As mentioned in section 6.1, all that matters is the relative distance in time between countries. Lockdown measures, vaccination programs, etc do not have to match, and the

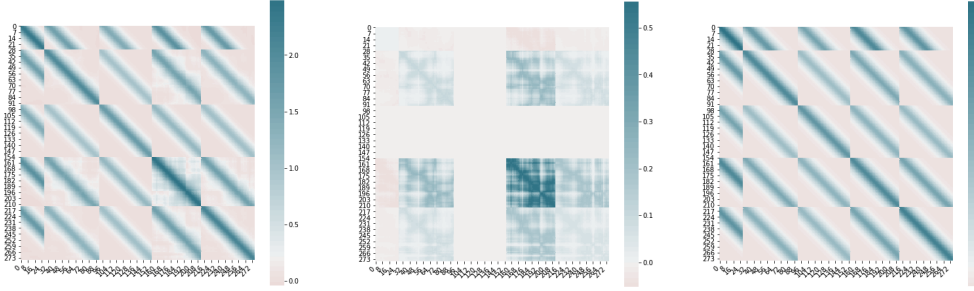


Figure 4: The figure on the left is the total variance \mathcal{K} as in (10), while the other two represent the component Kernel on the covariate space $B_1 \otimes K_{rbf}(\bar{X}, \bar{X})$ and time space $B_2 \otimes K_{Mat}(t, t)$, respectively

relationship between the main variable and lagged/forward version of the control units are still captured by the model, even if they are not linear.

Now, let us focus on the causal estimates. As shown in Figure 5, the GP model provides a close fit for the pre-intervention period. Following the beginning of the vaccination campaign, observations start to diverge from the counterfactual predictions: the actual number of weekly deaths, represented by the blue crosses, was consistently lower than what is predicted with slower vaccination rates. Subtracting observed from predicted data, as is shown on the right part of Figure 5 produces the posterior estimate of the effect achieved by the campaign. The top right graph gives an idea of the cumulative log number of deaths for the UK compared to control countries. Before the intervention the cumulative difference was statistically non-significant, i.e the differential number of deaths was the same among the countries. After t_0 however, the cumulative effect starts going down, reaching a value significantly lower than 0. In the UK the counterfactual (log) number of deaths was higher than the actual values, demonstrating that the vaccination campaign was effective in saving lives. The bottom right graph shows instead the point wise estimate of $\tau_{i,t}^*$, the multiplicative causal effect with 95% credible regions. To understand the average effect right after the campaign one can calculate the average effect as in (2). Over the whole period, on average, for every two COVID-19 deaths in the 4 countries used, there was one COVID-19 death in the UK (that is, the ratio $\bar{\tau}_i^*$ is 51.41% [30.05%, 82.86%]). In a Bayesian fashion, we also take into account parameter uncertainty, especially the one deriving from the coregionalization matrix B . In figure 5 the darker gray areas represent the supplemental uncertainty coming from parameter estimates, in particular due to the coregionalisation matrix.

6.2.2 Weekly infection rate R

The same analysis is run for the weekly infection rate, to measure if a different vaccination campaign is actually producing slower rates of infectiousness.¹³ Half of the selected countries selected ('Portugal' and 'Ireland') are in common with the previous analysis while 'France' and 'Denmark' are new control units. We can now employ type II Maximum likelihood on the whole data set to find the optimal hyper-parameters of the kernel. Given that the preproduction rate is an estimate itself, it can be affected by many sources of variability induced by the data or the model used. To take into account this effect, we bound the likelihood variance (observation error) to a minimum value of around 0.01, which corresponds to 5% of countries' reproduction rate variance over the observed period. In the Bayesian setting, we set up a slightly more informative prior $\omega_i^2 \sim \mathcal{G}(0.1, 1)$ to support the same decision. Without

¹³We removed the number of test variables as it did not affect results, making the optimization more challenging.

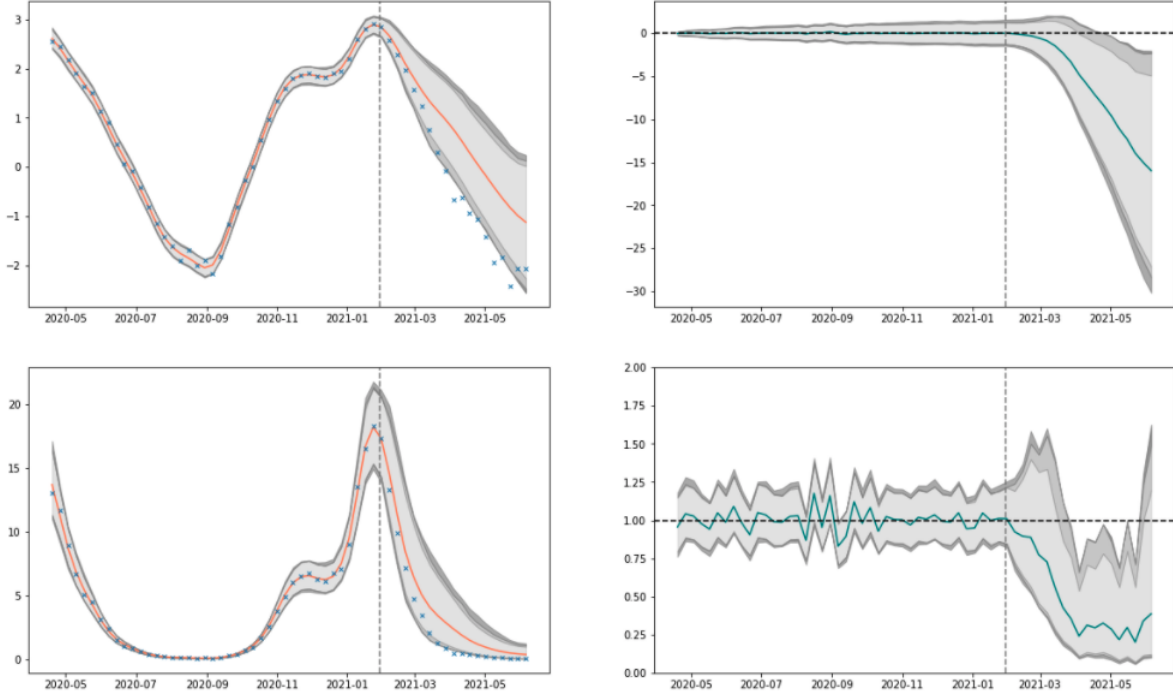


Figure 5: The graphs on the left indicate the log weekly deaths on top and the level on the bottom. Data provided to train the model is at the left of t_0 , the gray vertical line. Orange line represent model predicted average of (log) weekly death. True values are in blue. On the right part, the top graphs show the cumulative effect of log weekly deaths $T_{i,t}$ while the bottom display pointwise multiplicative causal effect $\tau_{i,t}^*$. Shaded area represent 95% credible intervals in gray. Light gray does not take into account parameter uncertainty, gray accounts only for λ and dark gray for λ and ω uncertainty.

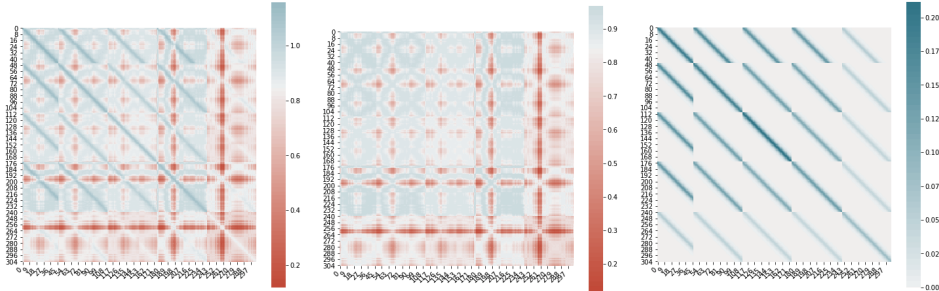


Figure 6: The figure on the left is the total variance K as in (10), while the other two represent the component Kernel on the covariate space $B_1 \otimes K_{rbf}(\bar{X}, \bar{X})$ and time space $B_2 \otimes K_{Mat}(t, t)$, respectively

these restrictions the model converges to a data representation with an almost zero observational error. This reflects in a tight in-sample fit but poor out-of-sample performances.

In contrast to the weekly number of deaths, the time component does not seem to play a prevailing role in defining R dynamics. Looking at Figure 6 one can note that there is mainly a contemporaneous effect, as the lengthscale ℓ of the Matérn kernel (7) is lower compared to the one estimated in 6.2.1. Decreasing the length parameter reduces the banding, as points further away from each other become less correlated. This means that data points have zero covariance with the lagged version of both the treated variable and control units. This effect is further minimized for ‘France’

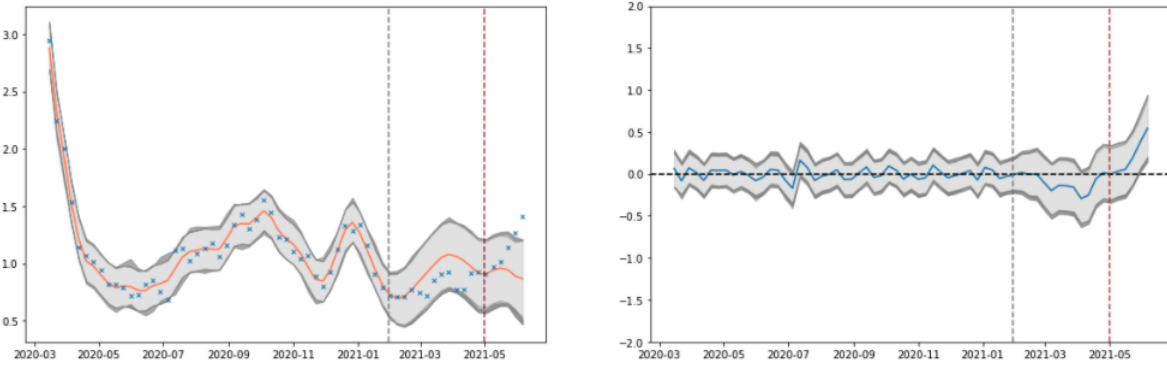


Figure 7: The graph on the left indicate the evolution of the reproduction rate in UK. Data provided to train the model is at the left of t_0 , the gray vertical line. The orange line represents the predicted average of R with 95% credible intervals in gray. True values are in blue. On the right part, the graph display point wise additive causal effect τ_t , with relative 95% bands in gray. The red vertical line at time '01-05-2020' indicates the start of the delta variant transmission in the UK.

(fifth country) as the estimate of $B_2^{[5,5]}$ is more than half the one of other countries. In contrast, Google mobility data, i.e. which places people were visiting during the period was effective in predicting how the contagiousness would change. However, as the variable is a principal component transformation, little interpretation can be given to single venues. The causal effect is then estimated on the available dataset. As shown in Figure 7, before the vaccination campaign the model provides a good fit of the data. Afterwards, counterfactual predictions (orange lines) initially follow the main trend of observed data but then they start to deviate marginally. However, the variability surrounding the estimate is too broad to confirm any causal effect in the data. It is interesting to note that in the very final period of the analysis, starting May 2021 (the red line in Figure 7), the model predicts a stable reproduction rate. However, the data seems to diverge positively to higher values. We suspect that reason for this discrepancy is the spread of the *delta* variant. This more contagious version of Covid-19 represented 73% of UK cases by the end of May 2021. Nevertheless, in the period following the vaccination campaign the average additive causal effect $\bar{\tau}_i$ equals 0.0063 with 95% credible interval [0.1653, -0.1582], thus no reduction is detected.¹⁴

7 Conclusion

A growing literature on applied causal inference indicates an increasing interest in evaluating the incremental impact of interventions and policies, especially during the COVID-19 pandemic (Li et al., 2021; Ma et al., 2022; Tang et al., 2022). With this paper, we propose a novel approach to obtain the counterfactual prediction of the unobserved outcome. We employ a Bayesian Machine Learning technique, based on Gaussian Processes, whose main features are discussed below.

The prevailing literature of dynamical Bayesian causal model revolves around Brodersen et al. (2014), whose approach is based on state-space models, which easily lend themselves to posterior inference. However, since closed-form solutions for the posterior are challenging to obtain, the authors resort to stochastic approximation, using MCMC.

¹⁴On the contrary, it is slightly positive, although not statistically significant

In the general form of Gaussian Processes, causal effect posterior evaluation can be instead derived analytically. When this is not possible - for example when using transformation of variables or cumulative measures - one can employ GP sampling procedure. As a GP is fully characterized by its mean (generally 0) and its variance (the kernel), the process is straightforward.

Furthermore, state-space models impose some restrictions on the dynamic evolution of the states, notably, linearity. With GPs, the input \mathbf{x} is transformed into a feature vector $f(\mathbf{x})$ through some non-linear mappings dictated by the structure of the kernel. In a time series, the degree of correlation between a variable and its lag is given by the relative time distance. When using a Matérn kernel, it can be shown that the covariance matrix of the kernel gives rise to a particular form of a continuous-time AR(p) Gaussian process (Rasmussen and Williams, 2006). At the same time, nothing prevents us from using a more complex structure - such as periodic, linear, etc., or a combination thereof - to better fit the time curve. Furthermore, the linearity assumption with exogenous regressors embodied in state space can be relaxed by adopting an appropriate kernel architecture. Machine Learning tools, such as cross-validation can help decide which one better describes the data.

Another important improvement that GPs put forward is an *heterotopic* configuration of data, i.e. each output has a different training set with a potentially different number of samples. This approach plays a crucial role in causal analysis since generally one has to discard all information after the intervention period to train the data, generating a non-negligible loss of data. In addition, no time matching is needed as the model understand the relationship among the potential outcome and the explanatory variables for each unit, independently if these variable match in absolute time.

Lastly using GPs one can easily quantify uncertainty around a measurement or prediction, since every data point possesses a defined distribution. This promotes direct estimation of the causal effect distribution, means, and quantiles.

To test this model in practice, we estimated the effect of the UK vaccination policy compared to other European countries. In particular, we analysed how the UK's faster inoculation campaign affected the cumulative number of deaths and the rate of contagiousness measured as by the reproduction rate. The results suggested that vaccinations prevented deaths, since on average, in the first semester of 2021, every death in the UK related to Covid-19 corresponded to two deaths in the rest of Europe. No statistically significant evidence was found to justify that vaccines reduce the number of cases directly caused by an infected individual. However, this has to be considered in light of the new and more infectious variants that started spreading over the continent at the end of our sample period.

References

Abadie, A., Diamond, A., and Hainmueller, J. (2010). Synthetic control methods for comparative case studies: Estimating the effect of California's tobacco control program. *Journal of the American Statistical Association*, 105(490):493–505.

Abadie, A. and Gardeazabal, J. (2003). The economic costs of conflict: A case study of the basque country. *American Economic Review*, 93(1):113–132.

Aglietti, V., Damoulas, T., Álvarez, M., and González, J. (2020). Multi-task causal learning with gaussian processes. In Larochelle, H., Ranzato, M., Hadsell, R., Balcan, M. F., and Lin, H., editors, *Advances in Neural Information Processing Systems*, volume 33, pages 6293–6304. Curran Associates, Inc.

Alaa, A. M. and van der Schaar, M. (2017). Bayesian inference of individualized treatment effects using multi-task gaussian processes. In Guyon, I., Luxburg, U. V., Bengio, S., Wallach, H., Fergus, R., Vishwanathan, S., and Garnett, R., editors, *Advances in Neural Information Processing Systems*, volume 30. Curran Associates, Inc.

Alvarez, M. A., Rosasco, L., and Lawrence, N. D. (2012). Kernels for vector-valued functions: a review.

Bojinov, I. and Shephard, N. (2019). Time series experiments and causal estimands: Exact randomization tests and trading. *Journal of the American Statistical Association*, 114(528):1665–1682.

Bonilla, E. V., Chai, K., and Williams, C. (2008). Multi-task gaussian process prediction. In Platt, J., Koller, D., Singer, Y., and Roweis, S., editors, *Advances in Neural Information Processing Systems*, volume 20. Curran Associates, Inc.

Born, B., Dietrich, A., and Müller, G. (2020). The lockdown effect: A counterfactual for Sweden. CEPR Discussion Papers 14744, C.E.P.R. Discussion Papers.

Brodersen, K. H., Gallusser, F., Koehler, J., Remy, N., and Scott, S. L. (2014). Inferring causal impact using Bayesian structural time-series models. *Annals of Applied Statistics*, 9:247–274.

Callaway, B. and Sant'Anna, P. H. (2021). Difference-in-differences with multiple time periods. *Journal of Econometrics*, 225(2):200–230. Themed Issue: Treatment Effect 1.

Cawley, G. C. and Talbot, N. L. C. (2007). Preventing over-fitting during model selection via bayesian regularisation of the hyper-parameters. *Journal of Machine Learning Research*, 8(31):841–861.

Chatzilena, A., Demiris, N., and Kalogeropoulos, K. (2022). A modelling framework for the analysis of the transmission of sars-cov2.

Djolonga, J., Krause, A., and Cevher, V. (2013). High-dimensional gaussian process bandits. In Burges, C. J. C., Bottou, L., Welling, M., Ghahramani, Z., and Weinberger, K. Q., editors, *Advances in Neural Information Processing Systems*, volume 26. Curran Associates, Inc.

Fletcher, R. (2000). *Newton-Like Methods*, chapter 3, pages 44–79. John Wiley & Sons, Ltd.

Gelman, A., Carlin, J. B., Stern, H. S., and Rubin, D. B. (2004). *Bayesian Data Analysis*. Chapman and Hall/CRC, 2nd ed. edition.

Ghayda, R. A., Lee, K. H., Han, Y. J., Ryu, S., Hong, S. H., Yoon, S., Jeong, G. H., Lee, J., Lee, J. Y., Yang, J. W., Effenberger, M., Eisenhut, M., Kronbichler, A., Solmi, M., Li, H., Jacob, L., Koyanagi, A., Radua, J., Shin, J. I.,

and Smith, L. (2020). Estimation of global case fatality rate of coronavirus disease 2019 (covid-19) using meta-analyses: Comparison between calendar date and days since the outbreak of the first confirmed case. *International Journal of Infectious Diseases*, 100:302–308.

Giorgino, T. (2009). Computing and visualizing dynamic time warping alignments in r: The dtw package. *Journal of Statistical Software*, 31(7):1–24.

Girolami, M. and Calderhead, B. (2011). Riemann manifold langevin and hamiltonian monte carlo methods. *Journal of the Royal Statistical Society: Series B (Statistical Methodology)*, 73(2):123–214.

Good, I. J. (1952). Rational decisions. *Journal of the Royal Statistical Society. Series B (Methodological)*, 14(1):107–114.

Her, P. H., Saeed, S., Tram, K. H., and Bhatnagar, S. R. (2022). Novel mobility index tracks covid-19 transmission following stay-at-home orders. *Scientific reports*, 12:7654.

Imbens, G. W. and Rubin, D. B. (2015). *Causal Inference for Statistics, Social, and Biomedical Sciences: An Introduction*. Cambridge University Press.

Jordan, A., Krüger, F., and Lerch, S. (2019). Evaluating probabilistic forecasts with scoringrules. *Journal of Statistical Software*, 90:1–37.

Li, Z., Xu, T., Zhang, K., Deng, H.-W., Boerwinkle, E., and Xiong, M. (2021). Causal analysis of health interventions and environments for influencing the spread of covid-19 in the united states of america. *Frontiers in Applied Mathematics and Statistics*, 6.

Liu, H., Cai, J., and Ong, Y.-S. (2018). Remarks on multi-output gaussian process regression. *Knowledge-Based Systems*, 144:102–121.

Ma, J., Dong, Y., Huang, Z., Mietchen, D., and Li, J. (2022). Assessing the causal impact of covid-19 related policies on outbreak dynamics: A case study in the us. *WWW '22*, page 2678–2686, New York, NY, USA. Association for Computing Machinery.

Matheson, J. E. and Winkler, R. L. (1976). Scoring rules for continuous probability distributions. *Management Science*, 22(10):1087–1096.

Menchetti, F. and Bojinov, I. (2020). Estimating the effectiveness of permanent price reductions for competing products using multivariate bayesian structural time series models. *Harvard Business School Working Paper*, 21-048.

Menchetti, F., Cipollini, F., and Mealli, F. (2021). Estimating the causal effect of an intervention in a time series setting: the c-arima approach.

Murphy, K. P. (2013). *Machine learning : a probabilistic perspective*. MIT Press, Cambridge, Mass. [u.a.].

Nocedal, J. and Wright, S. J. (2006). *Numerical Optimization*. Springer, New York, NY, USA, second edition.

Pearl, J. (1995). Causal diagrams for empirical research. *Biometrika*, 82(4):669–688.

Rasmussen, C. E. and Williams, C. K. I. (2006). *Gaussian processes for machine learning*. Adaptive computation and machine learning. MIT Press.

Rubin, D. B. (1974). Estimating causal effects of treatments in randomized and nonrandomized studies. *Journal of Educational Psychology*, 66:688–701.

Sävje, F., Aronow, P. M., and Hudgens, M. G. (2019). Average treatment effects in the presence of unknown interference.

Tang, W.-X., Li, H., Hai, M., and Zhang, Y. (2022). Causal analysis of impact factors of covid-19 in china. *Procedia Computer Science*, 199:1483–1489. The 8th International Conference on Information Technology and Quantitative Management (ITQM 2020 & 2021): Developing Global Digital Economy after COVID-19.

Tripathy, R., Bilionis, I., and Gonzalez, M. (2016). Gaussian processes with built-in dimensionality reduction: Applications to high-dimensional uncertainty propagation. *Journal of Computational Physics*, 321:191–223.

Zheng, C., Shao, W., Chen, X., Zhang, B., Wang, G., and Zhang, W. (2022). Real-world effectiveness of covid-19 vaccines: a literature review and meta-analysis. *International Journal of Infectious Diseases*, 114:252–260.